Eliminating VT uncertainties in modeling ferroresonance phenomena caused by single phase-to-ground faults in isolated neutral network

Zirka, S.E. ; Moroz, Y.I. ; Zhuykov, A.V. ; Matveev, D.A. ; Kubatkin, M.A. ; Frolov, M.V. ; Popov, M.

DOI
10.1016/j.ijepes.2021.107275

Publication date
2021

Document Version
Final published version

Published in
International Journal of Electrical Power & Energy Systems

Citation (APA)
Zirka, S. E., Moroz, Y. I., Zhuykov, A. V., Matveev, D. A., Kubatkin, M. A., Frolov, M. V., & Popov, M. (2021). Eliminating VT uncertainties in modeling ferroresonance phenomena caused by single phase-to-ground faults in isolated neutral network. *International Journal of Electrical Power & Energy Systems*, *133*, 1-12. Article 107275. https://doi.org/10.1016/j.ijepes.2021.107275

Electrical Power and Energy Systems 133 (2021) 107275

Contents lists available at ScienceDirect

International Journal of Electrical Power and Energy Systems

journal homepage: www.elsevier.com/locate/ijepes

Eliminating VT uncertainties in modeling ferroresonance phenomena caused by single phase-to-ground faults in isolated neutral network

S.E. Zirka [a], Y.I. Moroz [a], A.V. Zhuykov [b], D.A. Matveev [b], M.A. Kubatkin [b], M.V. Frolov [b], M. Popov [c,*]

[a] Dnipro National University, Faculty of Physics and Technology, Dnipro, Ukraine
[b] National Research University "Moscow Power Engineering Institute", Institute of Electrical Power Engineering, Moscow, Russia
[c] Delft University of Technology, Faculty of EEMCS, Mekelweg 4, 2628CD Delft, the Netherlands

ARTICLE INFO

Keywords:
Ferroresonance phenomena
Modes
Modeling
Voltage transformer

ABSTRACT

It is commonly recognized that correct transformer model (particularly topological one) is a key element for any ferroresonance simulations. This paper represents a line of reasoning by which a reliable model of a voltage transformer (VT) can be constructed given substantial uncertainties in its parameters and characteristics. Starting with catalog data for electric steels and typical leakage inductances of 6-kV VTs, a model of an isolated neutral network with three inductive VTs is initially fitted to reproduce in detail its ferroresonant behavior for a chosen network capacitance. Then, validity of the network model is verified by accurate predictions of ferroresonance processes for all other capacitance values available and thus different ferroresonance modes recorded during full-scale factory tests. Possibilities to simplify the VT model by neglecting dynamic, and then entire core losses and hysteresis are also shown.

1. Introduction

The list of network configurations and excitation scenarios fraught with ferroresonance phenomena seems almost endless [1]. Accordingly, there is an extensive literature on the subject [1–5], and there are no signs of its waning. A good literature review can be found in the multi-authored CIGRE brochure [3], which is a brief encyclopedia of the considered field. The continuing studies in this area corroborate the conclusions that "ferroresonance has never been well-understood" [1] and that "some unexplained breakdowns can be ascribed to this non-linear phenomenon" [5]. This causes interest in further ferroresonant studies, especially in those where the modeling is combined with careful experimentation. This paper falls into this category.

This work is devoted to modeling ferroresonance (FR) phenomena in ungrounded networks, which are in use, together with other network configurations, in China, Finland, Italy, Russia, Ukraine, etc. [6,7]. Their advantage is that the line-to-line voltages do not change during single line-to-ground (SLG) faults, which reach 80 percent of all faults in medium-voltage distribution networks. Because of this, no danger arises for the loads connected to the network, and its operation can be maintained for several hours under fault conditions.

The known disadvantage of the isolated neutral networks is ferroresonance overvoltages and overcurrents in electromagnetic voltage transformers (VTs), which can eventually result in their failures. Changes to other types of earthing are possible, but often have serious financial implications [6]. Therefore, attention is paid to the construction and operation of VTs, which, according to the valid standard [8], must withstand 8 h of continuous operation at 1.9 times the rated voltage.

During a short transient period following the fault occurrence (at, say, instant t_1 in Fig. 1), the voltages of the healthy phases increase to the line-to-line voltage level and remain at this level until the fault is cleared (at $t = t_2$).

Starting with instant t_2, voltage transformers of the network can resonate with its capacitances in certain, often unpredictable ways. In isolated neutral networks, most typical FR modes are the unbalanced fundamental mode and the quasi-periodic subharmonic 1/2 mode (QP-1/2) [4]. The latter is illustrated by the voltage waveforms in Fig. 1(a) and its magnified time window (TW) in Fig. 1(b). A close examination of Fig. 1(b) reveals an aperiodicity of the FR processes, so its 25-Hz designation is only used for convenience.

Transformer overcurrent in the mode QP-1/2 is illustrated by Fig. 2,

* Corresponding author.
E-mail address: M.Popov@tudelft.nl (M. Popov).

https://doi.org/10.1016/j.ijepes.2021.107275
Received 15 April 2021; Received in revised form 16 May 2021; Accepted 31 May 2021
Available online 4 July 2021

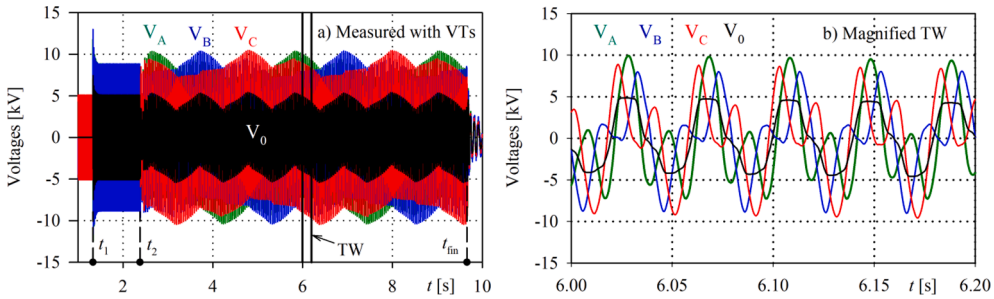

Fig. 1. a) Three-phase (V_A, V_B, V_C) and the zero-sequence (V_0) voltages measured in the presence of VTs and under FR conditions [9]; b) magnified time window (TW).

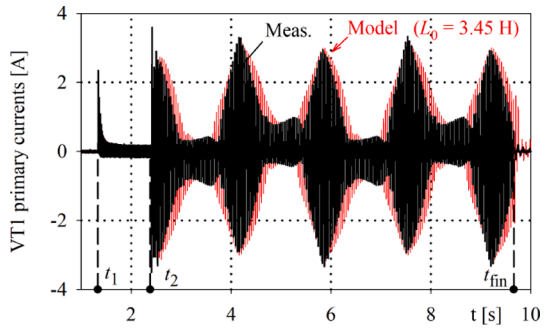

Fig. 2. Measured [9] and modeled currents of VT1 (phase A).

which shows the primary current in only one of the three VTs to avoid overloading the graph. During normal operation (at $t < t_1$), only a small magnetization current is drawn from the network. During the fault (at $t_1 < t < t_2$), the current amplitude is approximately tripled (after a short transient). Finally, when the resonance develops starting at $t = t_2$, the current takes the form of complex 25-Hz oscillations characterized by a low-frequency beat envelope seen in Fig. 2. Instant t_{fin} in Figs. 1 and 2 as well as in all the tests considered in the paper is the moment when the test bench is deenergized by its personnel.

Frequent SLG faults and economic losses brought on by subsequent FR processes gave rise to in-depth studies devoted to conditions of the parallel FR occurrence [5,7,10,11] and even larger literature on its prevention [12,13]. Nevertheless, a need in accurate full-scale experiments and their modeling are of utmost importance for understanding FR mechanisms and validating transformer model. To our knowledge, the experimental study reported in [9], is among the most thorough on the subject to date. The multiple intermittent SLG faults in [9] were carried out on a 6 kV experimental test bench operated by Ramensky Electrotechnical Plant Energy (RETZ Energy), Moscow Region, Russia. For completeness, several *metallic* faults at different network capacitances were also performed in the test bench. In the cases considered, the experimental test bench was equipped with a three-phase bank of single-phase three-winding VTs.

The fact that the ferroresonance can occur at different capacitance values of the same network points out that its reason lies in the magnetic nonlinearities of the transformer core. Therefore, the need for a reliable VT model is emphasized in many publications, starting with [2]. Even with detailed knowledge of transformer design and usual test results, an accurate modeling of all the FR modes observed in [9] would be a challenge. The modeling undertaken in this study was complicated by the absence of those data and by the fact that only fragmentary design information on the VTs employed was available. In particular, no information on the core material, leakage inductance or magnetization curve was provided. Besides, the variation of the total network capacitance was carried out by using different capacitors introduced into the network through an earthing transformer (ET) [14], which plays the role

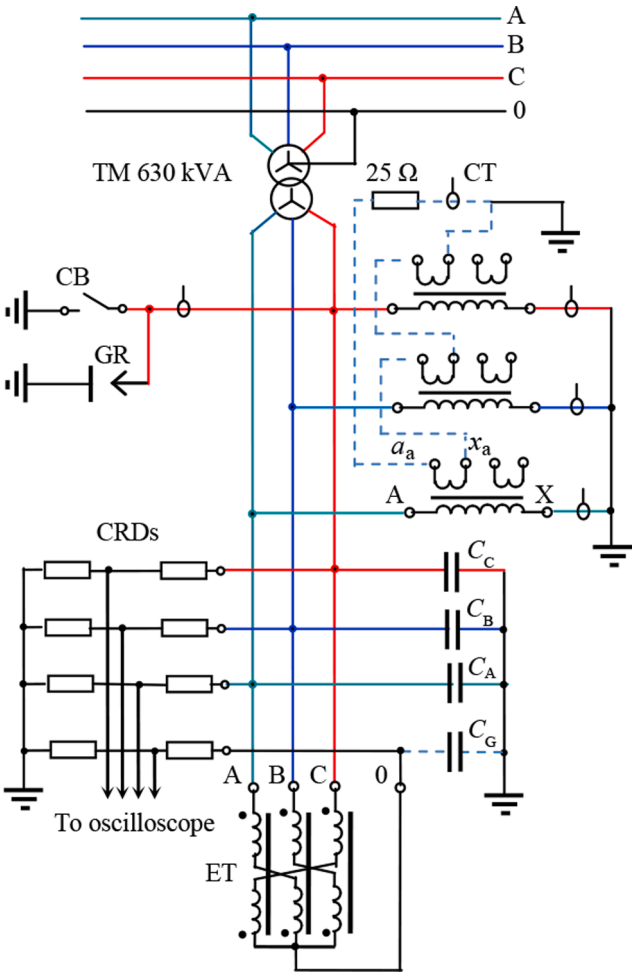

Fig. 3. Experimental setup arrangement.

of a zero-sequence filter [15]. Therefore, this electromagnetic apparatus should also be included in the test bench model.

Two model features, often mentioned in studying resonance phenomena, is the involvement of hysteresis [16–20] and the influence of nonlinear core loss dependencies on voltage and frequency [21,22]. It should be noted, however, that the role of these factors is mainly discussed when simulating *series* ferroresonant circuits [1,23], in which the transformer is fed through a series capacitor [21].

In the *parallel* mid-voltage circuits, such as that considered in this paper, the role of core loss is evaluated differently. For example, it is concluded in [24] that computed results are closer to experimental observations if core losses are included in the model. On the contrary, the impact of a large (megaohm) loss resistance, placed in parallel with the

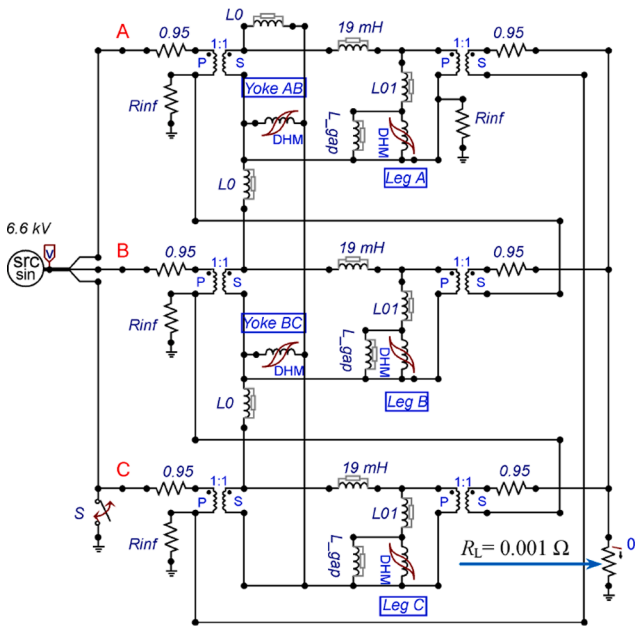

Fig. 4. ET model used in short circuit analysis.

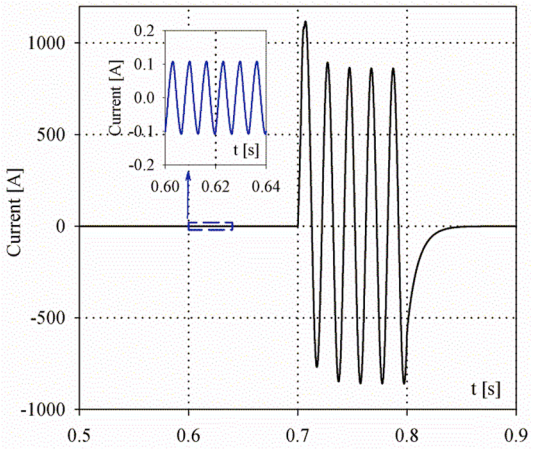

Fig. 5. Short circuit current in the ET neutral.

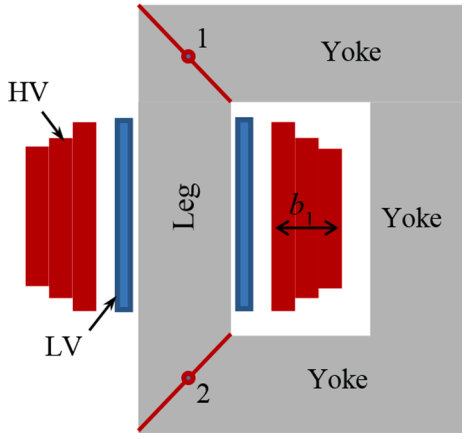

Fig. 6. Voltage transformer arrangement.

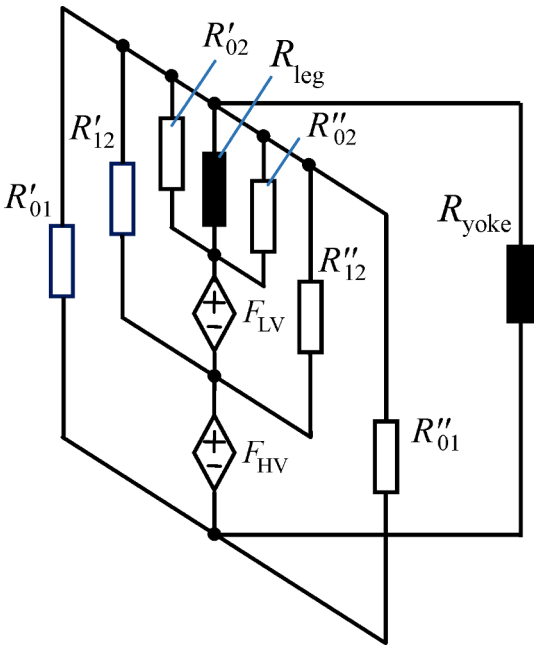

Fig. 7. Magnetic circuit of the VT in Fig. 6.

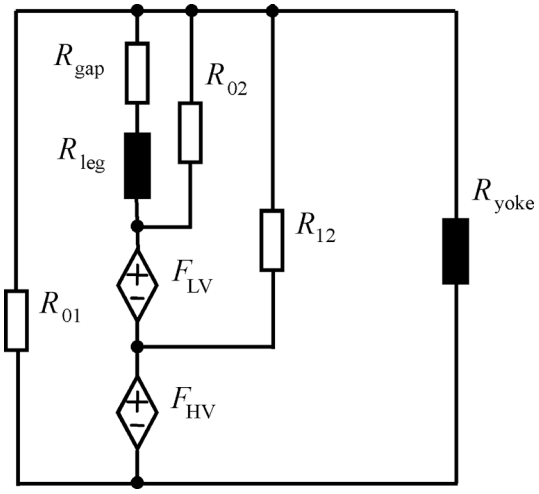

Fig. 8. Reduced magnetic model of the VT.

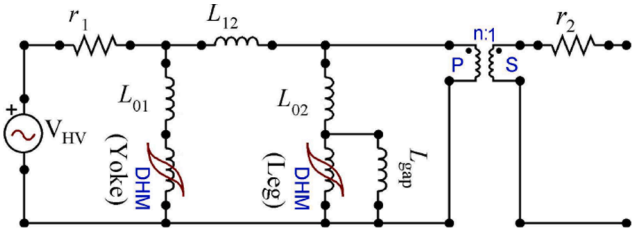

Fig. 9. Electric π model of the VT employed.

magnetizing inductance, seems insignificant. That led to the conclusion about a negligible effect of core losses on the ferroresonance damping [5]. The impact of hysteresis was not studied at all, as applied to *parallel* ferroresonant circuits. This situation requires clarification and suggests performing physical and numerical experiments, in which the core topology would also be taken into account, as suggested in [1].

First, a full (lossy and hysteretic) VT model is developed, which

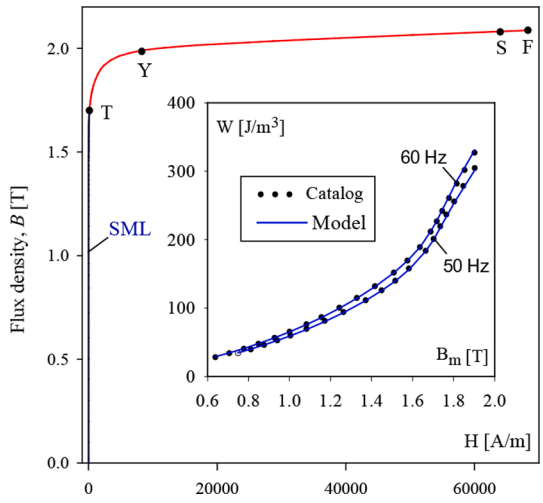

Fig. 10. Saturation curve and loss characteristics of Steel M5.

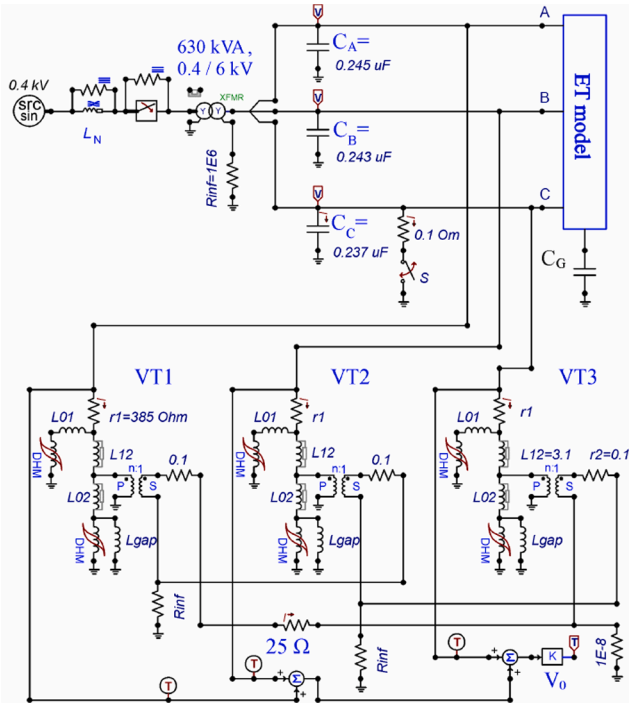

Fig. 11. Model of the test bench.

Table 1
Metallic faults recorded/modeled.

Test	C_0 [μF]	Delta	FR mode
1	2.19	Broken	≈ 25 Hz
2	2.19	With 25 Ω	≈ 25 Hz
3	1.44	Broken	Chaotic
4	1.44	With 25 Ω	No FR

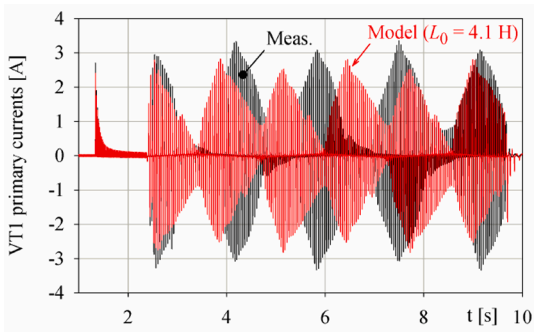

Fig. 12. Primary current in VT1 predicted with an untuned model.

Table 2
Inductances of VT models.

Core model	L_{12} [H]	L_{02} [H]	L_{gap} [H]
DHM-based	2.3	1.15	550
SHM-based	2.4	1.20	400
Lossless	2.5	1.25	400

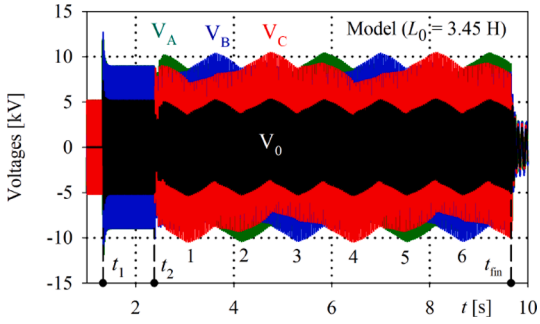

Fig. 13. Replicated low-frequency beats.

reproduces accurately all the experimental FR modes recorded in [9]. Then, the VT model is simplified sequentially by removing dynamic and, finally, its quasi-static (hysteretic) component. Comparative results of this study are discussed in Section 5 of the paper.

2. Test bench and its elements

2.1. Test bench arrangement

The experimental setup in Fig. 3 is fed from a step-up Yyn0 630 kVA transformer, which increases the voltage of the local utility grid (0.4 kV, 50 Hz) to 6 kV. The isolated network condition of the test bench is caused by ungrounded transformer neutral on its 6 kV side.

The primary rated voltage V_1 of three epoxy-cast VTs is $6000/\sqrt{3}$ V. The main secondary windings (used for metering and protection purposes) are open-circuited and their effects are ignored when considering ferroresonance. The auxiliary secondary windings (a_a-x_a) with voltage $V_2 = 100/3$ V are connected in the broken delta and can be optionally loaded with a damping resistor of 25 Ω.

Single-phase faults are carried out by switching a vacuum circuit breaker (CB) directly to the test bench grounding grid (metallic fault) or by multiple touching/detouching a grounding rod (GR) when imitating arcing faults [9].

The digital oscilloscope registers signals from capacitive-resistive dividers (CRDs). Current transformers (CTs) are used extensively for monitoring the operation of the test bench.

Three capacitors with capacitances $C_A = 0.25$ μF and

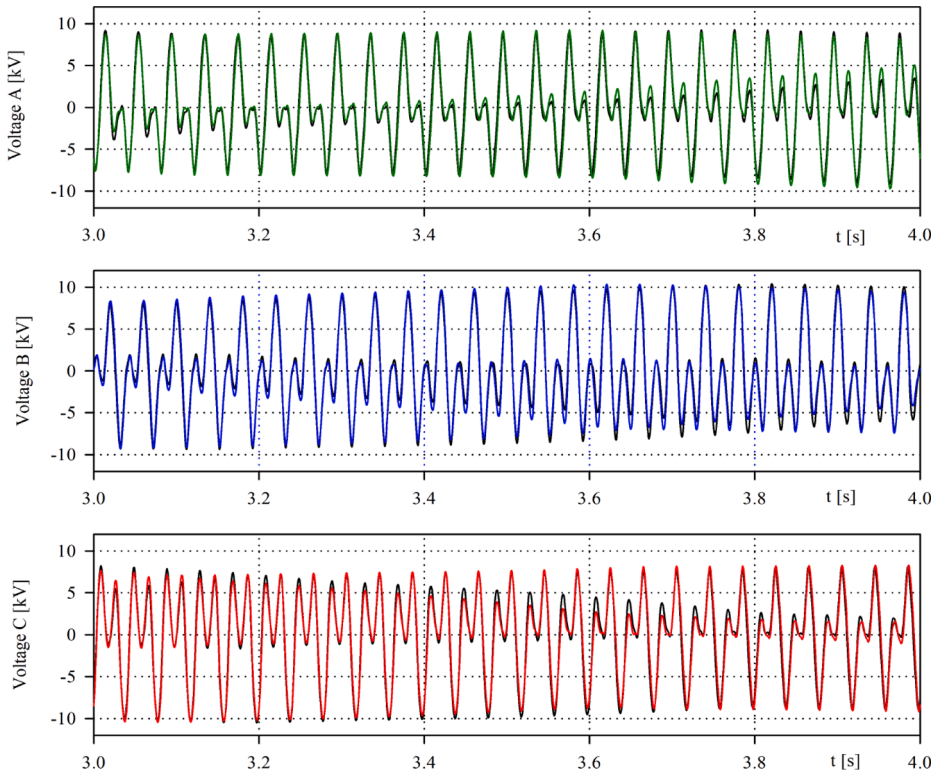

Fig. 14. Calculated waveforms of phase voltages V_A, V_B, and V_C (colored lines) superimposed on the measured ones (black lines).

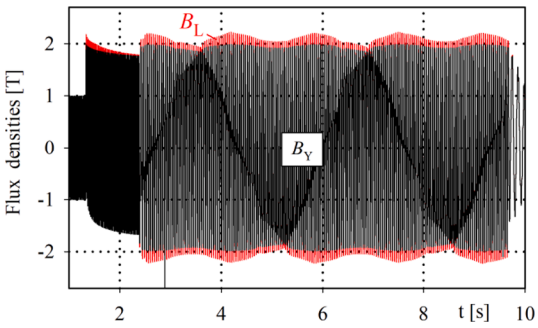

Fig. 15. Flux densities in the leg and yoke of VT1.

$C_B = C_C = 0.24$ μF form minimum capacitance, $C_{min} = C_A + C_B + C_C = 0.73$ μF, which is an irreducible (permanent) capacitance, involved in all the tests analyzed below. When the total capacitance should be increased above C_{min}, an additional capacitance C_G is connected between the ungrounded ET neutral and the grounding grid of the setup. In this case, the zero-sequence capacitance of the test bench is determined as $C_0 = C_{min} + C_G$. To enable observation of all possible FR modes, the fuses were removed from all VTs and the experimental timings were chosen so as to prevent damage to the transformers.

2.2. Topological model of the earthing transformer

The ET in Fig. 3 is an earthing transformer [14], which is usually employed for creating a neutral point in ungrounded, three-phase systems. The ET is a zig-zag, core-type apparatus having three legs similar to those of a power transformer [15]. Each leg is wound with two equally-spaced concentric windings (half-windings) connected to different lines. So, the leg is magnetized by a vector sum of two 120-degrees phase-shifted voltages. The upper dotted terminals of the ET in Fig. 3 are starts of the *outer* windings, while the dotted starts of the *inner* windings form the ET neutral point 0.

The close design similarity between the ET and a usual core-type transformer, allows one to use existing topological models of two-winding, three-phase transformer, for example, the electric transformer model detailed in [25]. The presence of six ideal transformers (ITs) in such a model makes it universal in the sense that delta, wye, or zig-zag winding connection can be made *outside* of the model of the core equivalent. A properly simplified transformer model from [25] with the windings configured to reproduce the ET operation is shown in Fig. 4.

Five hysteretic inductors represent magnetic paths in the legs and yokes, and users of ATP and ATPDraw can employ, starting from 2020, the library Type-96 DHM inductors, which implement a dynamic hysteresis model (DHM) [26]. Linear inductances L_{01} (=0.2 mH) take into account the non-magnetic gap between the inner windings and legs; resistors (0.95 Ω) represent resistances of half-windings, and 19 mH are their leakage inductances. Inductances L_{gap} (=15.8 H) represent the core gaps between the legs and yokes assumed to be 0.25 mm. Inductances L_0 (=0.4 mH) characterize off-core zero-sequence paths. A three-phase ramped voltage is initially applied to the ET model to perform its accurate initialization.

According to [27], maximum currents will flow through ET windings when its neutral and one of the phase terminals are grounded simultaneously. This special "short circuit" mode can be reproduced in the scheme of Fig. 4 by closing switch *S*. Fig. 5 shows the current in the neutral (with a negligibly small resistance R_L) computed for the case when switch *S* is closed at $t = 0.7$ s and opened at $t = 0.8$ s. It can be seen in the magnified inset that prior to closing switch *S*, that is, at $t < 0.7$ s, the 150-Hz neutral current of the ET is quite small, despite the grounded neutral. The RMS and peak current values obtained with the model in Fig. 4 are close to those provided by the manufacturer [27].

2.3. Topological model of voltage transformer

It was recognized from the very beginning that the model of voltage

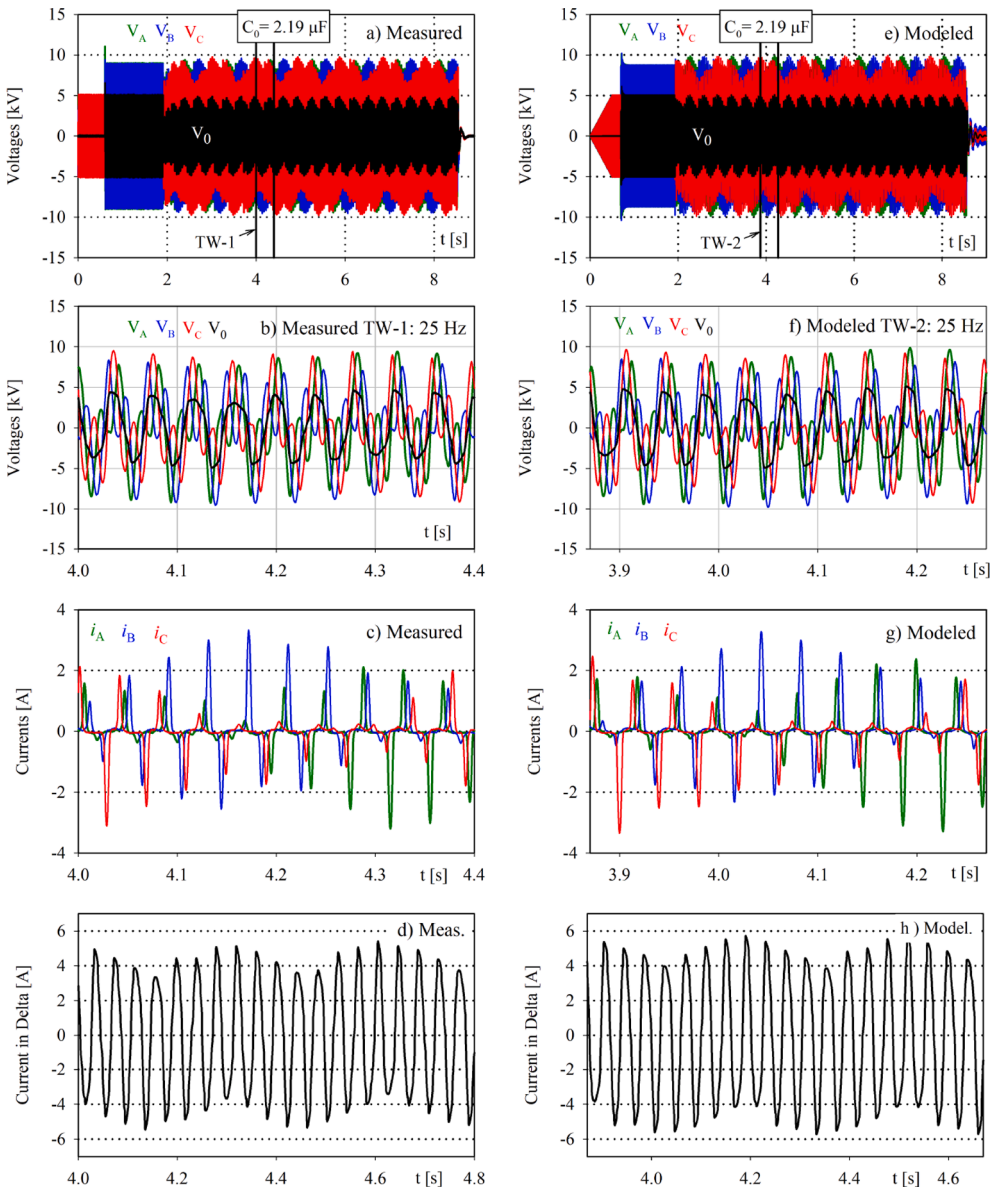

Fig. 16. Measured (a, b, c, d) and computed (e, f, g, h) waveforms at $C_0 = 2.19$ μF and closed delta connection.

transformer can be crucial in ferroresonance studies [28]. Similar to inrush current events, the most influential feature of the VT's behavior under ferroresonant conditions is the saturation of its core (a part of the core). Although appropriate transformer models were recently discussed in [29], it is still worthwhile to return here to modeling a single-phase, core type transformer.

To make the discussion concrete, assume that three-winding VT has a construction shown in Fig. 6 where the auxiliary low voltage (LV) winding is the inner one, the three-layer high voltage (HV) winding is the outermost, and the empty space between them is the place occupied by the main LV winding and necessary interwinding insulation. As this "middle" winding is open-circuited, it is not shown in Fig. 6 and is not a matter of consideration.

Following [30,31], it is assumed that the modeled core can be divided in *two* parts. Taking into account the space position of the windings in Fig. 6, it is natural to place the nodes 1 and 2 of the magnetic circuit on the axis of the leg. This subdivides the core into the leg and the return yoke, where the latter covers two horizontal branches and the end limb, as shown in Fig. 6. In the transformer magnetic model of Fig. 7 these core parts are represented by hysteretic reluctances of the leg (R_{leg}) and yoke (R_{yoke}).

The mentioned core subdivision is in accordance with that employed for decades in the inrush current evaluation [30] where the current peak in a single phase transformer is estimated using its saturation inductance

$$L_{sat} = \frac{\mu_0 N^2}{h} \times \frac{\pi d_{eq}^2}{4} \tag{1}$$

Here h is the height of the exited winding or core window, while the equivalent diameter d_{eq} is determined by the diameter of its mean turn [32] or is found as $d_{\text{eq}} = d_{\text{in}} + 2b_1/3$ [33] where d_{in} is the inner diameter of the winding and b_1 is its thickness.

Although somewhat different values of h and d_{eq} have been reported in the literature (see [32] for details), there is nothing mention about the yokes in (1). This means that (1) refers to the winding encircling a completely saturated leg, which is positioned between two *unsaturated* (or much less saturated) yokes [30].

The saturation of the yoke is restrained by the presence of the off-core flux paths (characterized collectively by reluctance R_{01}) which, compared to the yokes, have shorter lengths and larger cross sections. Unlike relatively "flat" flux paths in the leg and yoke, reluctance R_{01} is

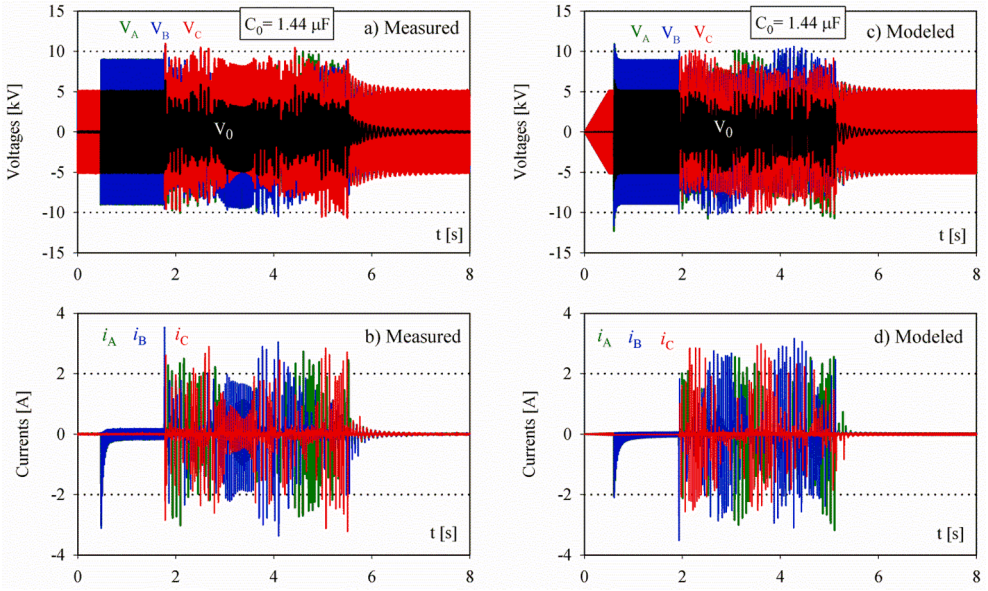

Fig. 17. Measured (a, b) and modeled (c, d) waveforms at $C_0 = 1.44$ μF.

Table 3
Arching faults recorded/modeled.

Test	C_0 [μF]	FR mode	Probability
5	4.8	≈ 25 Hz	17/21
6	2.2	≈ 25 Hz	18/23
7	0.73	50 Hz	4/20

distributed in space. To stress this feature, it is represented in Fig. 7 by two (of many) parallel branches (R'_{01} and R''_{01}). In the same manner, Fig. 7 shows the distributed reluctance R_{12} of the leakage channel and reluctance R_{02} of the channel between the LV winding and the leg. Finally, the sources of magneto-motive force (MMF) F_{HV} and F_{LV} in Fig. 7 represent the HV (outer) and LV (inner) windings, respectively.

Usually, the scheme in Fig. 7 is depicted in its normal "flat" configuration shown in Fig. 8, which can be supplemented with a linear reluctance R_{gap} representing the air gap(s) in the core.

A strict (duality derived) electric equivalent of this magnetic model is shown in Fig. 9 where DHM-inductors represent the leg and yoke. The subscripts of the linear inductances L in Fig. 9 are the same as those of the linear reluctances R in Fig. 8. These values are linked by the relationship $L = N_1^2/R$ where N_1 is number of turns in the *outer* HV winding. To link the model to LV circuits, it is supplemented by an ideal transformer with a turns ratio $n = V_1/V_2$ (=104). Therefore, r_1 and r_2 are real (non-referred) resistances of the primary and secondary windings.

Except for resistivity r_1 (=385 Ω), no other electromagnetic parameters were measured on the stand-alone VT. Partial VT disassembly allowed estimating the lengths of the leg and yoke as 0.17 and 0.476 m, respectively. Cross sectional area of the core was assessed to be 0.002475 m^2, and the number of turns in the auxiliary inner winding is 64. So the HV winding should contain about 6650 turns and the flux density in the core is near 1.0 T under normal operating conditions. The gap in the core was chosen to be 0.25 mm that yields inductance L_{gap} of 550H.

In the absence of any magnetization curves, the core material may be chosen from catalogs or among 12 grain-oriented (GO) steels, both conventional and high permeability (HiB), contained in the catalog-based DHM library. Numerical experiments carried out using these steels have inclined us to think that core material is a conventional GO steel similar to M4 or M5. For definiteness, and to reduce the number of unknown parameters, the latter steel was chosen to be used in the VT model.

In addition to hysteretic characteristics, an important element of any dataset of the DHM library is its saturation curve. Fig. 10 shows such a curve T-Y-S-F taken from Armco catalog [34] for GO steel M5. This single-valued curve is an extension of the static major loop (SML) to the level of "technical saturation", which is estimated, depending on the steel, in the range of 1.96 to 2.06 T. The slope of the last segment S-F of curve T-Y-S-F is equal to the vacuum permeability μ_0. This fact requires introducing inductances L_{01} and L_{02} in the leg and yoke branches of the model in Fig. 9. Among them, inductance L_{02} is the main element controlling the *final slope* of the magnetization curve, which is widely used in inrush current estimations.

It is remarkable that ascending and descending branches of the SML are indistinguishable in the scale of Fig. 10. The interested reader can find hysteresis loops of steel M5 in [26].

The inset of Fig. 10 shows catalog (dots) and modeled (lines) loss curves of steel M5 evaluated at sinusoidal flux densities for 50 and 60 Hz. The shape of these curves illustrates the nonlinear dependencies of specific loss on voltage and frequency mentioned in advanced ferroresonance literature.

In terms of the model in Fig. 9, a lesser saturation of the yoke is due to the fact that inductance L_{01} is appreciably greater than both the leakage inductance L_{12} and the small inductance L_{02} of the innermost channel. For this reason, the feeble-current branch L_{01} – *Yoke* is often omitted in VT representations, and simplified Γ-type transformer models are mainly used in ferroresonant studies [5,35].

These black-box models can be acceptable when their parameters are fitted to measurements covering high flux densities in the core. However, remembering different saturation levels of the leg and yoke, there is no definite answer as to determining parameters of the single magnetization branch of these Γ-models starting from *B-H* curves of a given material. Therefore, it was decided to use the π-type model represented in Fig. 9. Relying on results provided in [29,30] the ratio L_{01}/L_{12} can be chosen in the range of 10 to 20 for the applied small VT. The choice L_{12} and L_{02} is explained in Section 3.1.

3. Fitting the test bench model to measurement data

With the use of the VT model in Fig. 9, the model of the test bench as a whole takes the form shown in Fig. 11.

It was pointed out in [28] that the source representation is not

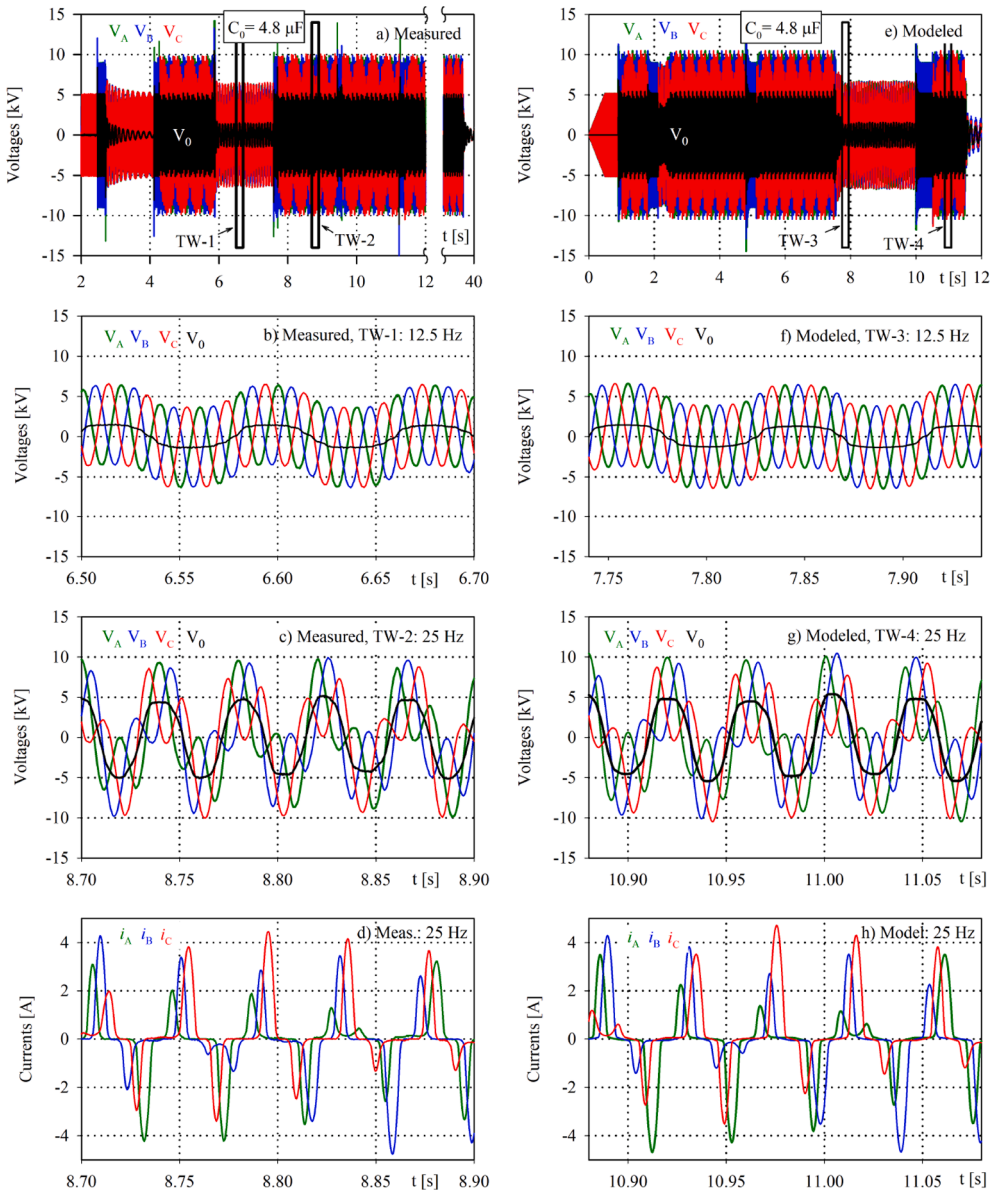

Fig. 18. Measured (a, b, c, d) and modeled (e, f, g, h) waveforms at C_0 = 4.8 μF.

critical, unless the source contains nonlinearities. Although the 630 kVA supply transformer does contain magnetically nonlinear elements, it was found that both its topological DHM-based model (similar to that in [25]) and the XFMR model [36], shown in the compact form in Fig. 11, yield the same results. The 630 kVA transformer employed in the model is characterized by per-phase leakage inductance of 8.6 mH and short-circuit resistance of 0.76 Ohm, both referred to the 6 kV side. Besides, the referred per-phase inductance L_N of the 0.4-kV network was estimated to be 10 mH.

The zero-sequence voltage, $V_0 = (V_A + V_B + V_C)/3$, is calculated by consecutive summation of the line-to-ground voltages (V_A, V_B, and V_C), and then by multiplying the sum by 1/3 using the TACS component K.

When the 25-Ω resistor should be excluded, all three ideal transformers are omitted in the model. In this case, inductances L_{12} and L_{02} in each of VT models are merged in a single inductor L_0, which is the main fitting parameter of the model.

It was found advisable to start the VT modeling by replicating ferroresonance phenomena caused by removing *metallic* SLG faults. As a first step, FR processes recorded at the broken delta winding (Test 1 in Table 1) were to be modeled with pinpoint accuracy. The same accuracy should then be maintained when the delta winding is closed with the 25-Ω resistor provided (Test 2) and another network capacitance is employed (Tests 3 and 4). In Section 4, the model is further verified against experimental data recorded during repetitive arching SLG faults.

3.1 A single SLG metallic fault with C0 = 2.19 μF and broken delta secondary (Test 1)

As explained previously, inductances L_{12} and L_{02} are merged, in this case, into a single inductance L_0, which is the main adjustable parameter of the model. Its order of magnitude can be estimated by orienting towards the range of short-circuit voltages of 6-kV VTs [37], which vary from around 3% to 5%. For the VT with a maximum rating of 630 VA, this yields the leakage inductance L_{12} in the range between 1.3 and 2.2H. To evaluate L_0, this value should be increased to take into account the thickness of the LV winding and the width of the innermost gap. This gap is not negligible because it includes a large empty space between the circular LV winding and a non-circular (staircase) shape of the leg's cross section. So the value of L_0 could be expected in the range of

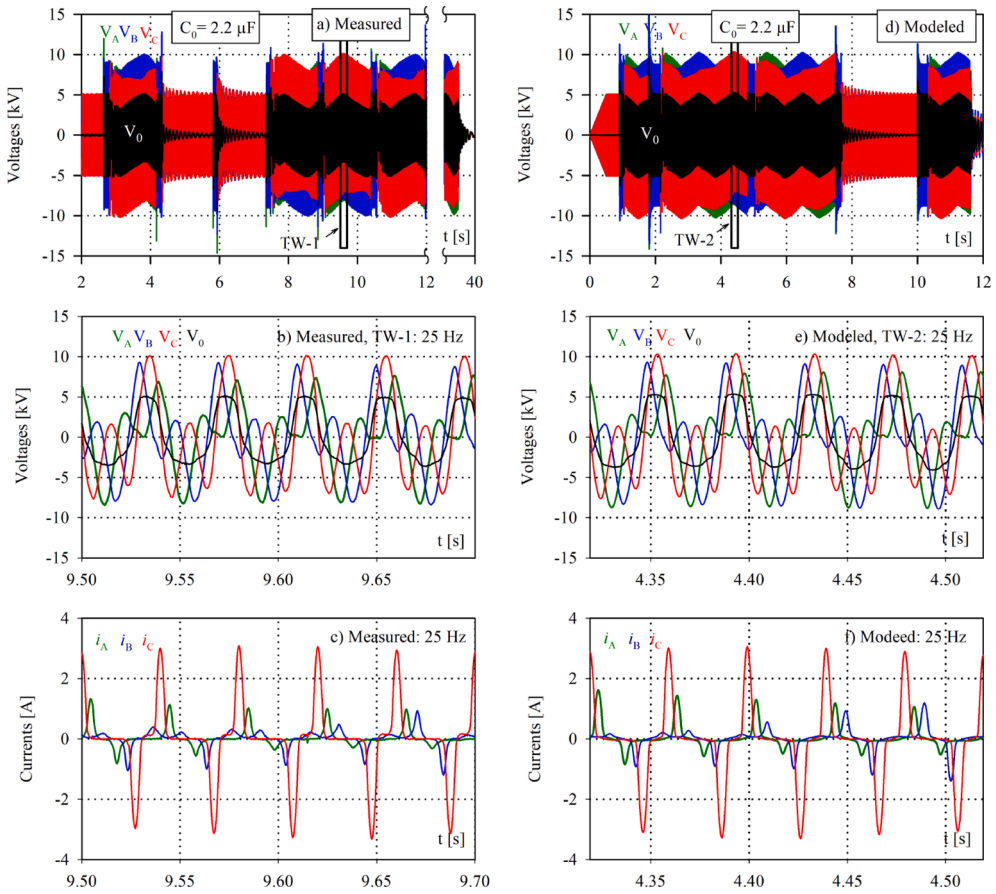

Fig. 19. Measured (a, b, c) and modeled (d, e, f) waveforms at $C_0 = 2.2$ μF.

approximately 3.1 H–4.1 H. The value of L_{01} can be taken equal to 20 H to be one order of magnitude larger than L_{12}. A small number of steps in the core cross section, typical of low-voltage VTs, increases, as mentioned, the gap between the inner winding and the leg. This allows us to set the ratio L_{02}/L_{12} (that is the proportionality factor K) equal to its typical value of 0.5 [36].

The test discussed in this sub-section was made for $C_G = 1.46$ μF placed in the neutral of the ET. The primary current of transformer VT1 calculated with the model for $L_0 = 4.1$ H, i.e. for the upper boundary of the mentioned interval [3.1, 4.1] H, is shown in Fig. 12.

As seen from Fig. 12, the current peaks calculated for $L_0 = 4.1$ H are markedly lower than the measured ones. This means that inductance L_{sat}, determined by (1), should be decreased, which is achieved by decreasing diameter d_{eq}. In the physical meaning, this decreases the leakage inductance L_{12}, and hence the sought inductance L_0. Using the try-and-error approach, it can be found that the calculated peaks become close to measured ones at $L_0 = 3.45$ H, as shown in Fig. 2. With the chosen value of K (=0.5), this gives $L_{12} = 2.3$ H and $L_{02} = 1.15$ H entered in the first row of Table 2.

It is remarkable that, in this case, the beat frequency of the computed current is in reasonable agreement with the measured value. The same agreement is observed between the computed voltages shown in Fig. 13 and the measured voltages in Fig. 1(a), which have the same number of peaks in their envelopes (6 ½) and are of exactly the same shape (coloration).

The complex voltage waveforms in Fig. 13 can only be examined in sufficient detail within an extended time window. In the one-second time interval of Fig. 14, the calculated waveforms of phase voltages A, B, and C are superimposed on the measured ones. By taking into account some distortions (nonsinusoidality) of the mains voltage waveforms, the coincidence of the curves in Fig. 14 is almost perfect.

An additional indicator of the model validity is the practical coincidence of the computed (24.850 Hz) and measured (24.851 Hz) frequencies of the zero sequence voltage V_0, which were found using subsequent Fourier analysis.

In concluding this subsection, it is instructive to compare, in Fig. 15, flux density waveforms in the yoke (B_Y) and leg (B_L) of, say, transformer VT1. Their close examination reveals that crests of B_Y never exceed the value of 1.985 T, which is marked by point Y in Fig. 10. By contrast, the maxim value of B_L (=2.216 T) lies far to the right of point F, as could be expected.

As shown in [38] and [39, Section 6.6.2], different flux densities in the yoke and leg are observed experimentally in transformers of different types and ratings. Together with the indivisibility of the leakage inductance, this necessitates the use of the π equivalent circuit employed in this study.

3.2. A single SLG metallic fault at $C_0 = 2.19$ μF ($C_G = 1.46$ μF) and 25-Ω resistor completing the broken delta circuit (Test 2)

A widely used method of preventing FR in isolated neutral network is to close the broken delta through a resistor (typically of 25 Ω). The measured and computed waveforms provided in Fig. 16 show that this method is not effective, contrary to what could be initially expected.

Regarding the modeled waveforms, Fig. 16 shows their good agreement with the measured curves. This relates to both the voltage and current waveforms. Paying attention to both is important because the medium voltage VTs can be damaged from both overvoltages and, more often, current overheating [9]. Besides, the modeling reveals that the current waveforms are more sensitive to changes in model parameters than the voltage curves.

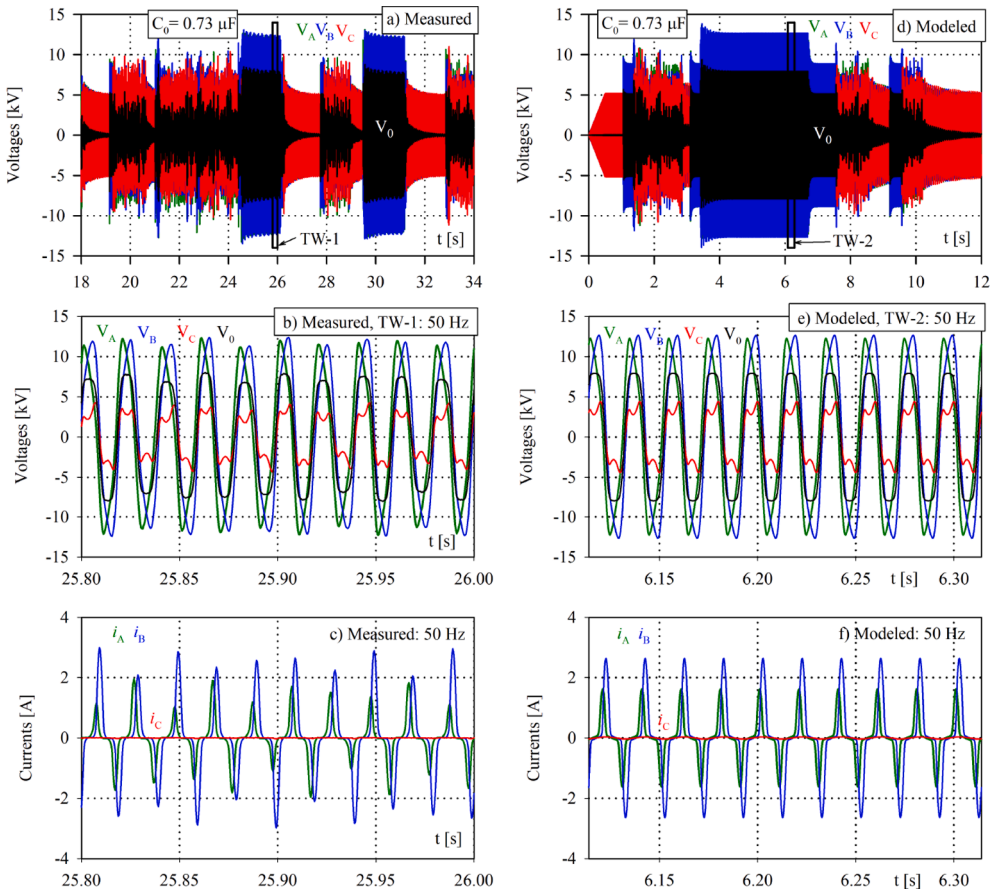

Fig. 20. Measured (a, b, c) and modeled (d, e, f) waveforms at $C_0 = 0.73$ μF.

3.3. A single SLG metallic faults with $C_0 = 1.44$ μF (Tests 3 and 4)

The case with the broken delta secondary is characterized by chaotic FR oscillations, Fig. 17(a), which die out into the normal operating mode at unpredictable instant. In the modeling, such an instant was chosen so that the computed waveforms in Fig. 17(c) and (d) were similar to those in Fig. 17(a) and (b).

Regarding comparison of the calculated and measured processes in Fig. 17, it should be noted that chaotic modes are characterized by a highly irregular behavior, so it is difficult to expect that any model would predict chaotic oscillations in smallest details.

When the delta is closed through the provided 25-Ω resistor (Test 4), the model does not predict any noticeable resonance despite a short-term saturation of all three VTs can sometimes occur immediately after opening the CB.

4. Testing the model at multiple repetitive SLGs

To imitate intermittent arcing faults, three tests with repetitive SLGs were performed using the test bench with the broken delta secondary and network capacitances pointed out in Table 3. From 20 to 23 faults on phase C to ground were applied and removed during approximately 40 s using the grounding rod, GR, designated in Fig. 3. The probability of the predominant FR mode in Table 3 is the ratio of its occurrences to the total number of SLG in a given test.

Because of the unpredictable nature and drastic changes in the arc behavior [40], we suspended attempts of its accurate modeling. Instead, it was found acceptable to use a resistance (0.1 Ω) in series with switch S, as shown in Fig. 11.

4.1. Test with 21 consecutive SLG faults with $C_0 = 4.8$ μF (Test 5)

When a capacitor with $C_G = 4.075$ μF is included in the neutral of the ET then, taking into account the permanent capacitances C_A, C_B, C_C of the test bench, its zero sequence capacitance is 4.8 μF. It was observed in the test detailed in [9, Fig. 7] that out of 21 consecutive *events* (when the SLG is applied and removed), 17 were followed by quasi-periodic subharmonic oscillations with a frequency slightly less than 25 Hz (1/2 mode). Three *events* were accompanied by fast resonance decay and recovery to the normal steady-state operation, and only a single event has led to the 1/4 resonance mode of 12.5 Hz. So, the 1/2 mode FR is obviously *dominant* at $C_0 = 4.8$ μF. This is consistent with the early observation in [2] that "dividing lines between distinct modes of instability are not very clear-cut." The blurring of these lines can be explained by various point-on-wave switching operations and thus various remanent flux densities in the cores of all three VTs.

A first third of the entire process, measured in [9], is shown in Fig. 18(a). Two time windows (TW-1 and TW-2) are chosen to show in more detail the single 1/4 mode (in Fig. 18(b)) and the predominant 1/2 mode in Fig. 18(c) and (d).

The same behavior is exhibited by the model in Fig. 11. From six SLG events represented in Fig. 18(e) four were followed by the 1/2 mode FR, and only a single one initiated the 1/4 resonance mode. It should be noted that lots of attempts were required to capture this unrepresentative mode by varying the instant of the SLG clearance after the fourth fault in Fig. 18(e).

As can be seen in Fig. 18(f), (g), (h), the modeled processes in time windows TW-3 and TW-4 show a good correspondence with those in windows TW-1 and TW-2.

4.2 Test with 23 consecutive faults with C0 = 2.2 μF (Test 6)

With a capacitor C_G = 1.475 μF included in the neutral of the ET, the zero sequence capacitance of the network is 2.2 μF. It was reported in [9, Fig. 9] that 18 out of 23 consecutive SLG events, were followed by quasi-periodic subharmonic oscillation of 25 Hz (1/2 mode), and five events were accompanied by the recovery to the normal steady-state condition. A first third of the process, measured in [9], is shown in Fig. 19(a) where time window TW-1 is used to show the prevalent FR mode in detail. Both these behaviors were easily reproduced in the modeling of five successive SLG, as shown in Fig. 19(d). This fact and the probability of 18/23 (in Table 3) show that the 25-Hz oscillations are typical for this network capacitance.

4.3. Test with consecutive faults with the minimum network capacitance, C_0 = 0.73 μF (Test 7)

At a minimum network capacitance (C_0 = 0.73 μF), 20 consecutive SLG events were carried out. Two of them were followed by sustained chaotic FR processes, 14 events have led to quenched oscillations, and only after four events a stable 50-Hz FR was observed with a small current in the primary of the VT of phase B. A part of the measured events is shown in Fig. 20(a) with enlarged voltages and currents recorded during time window TW-1, see Fig. 20(b) and (c).

Because of its low probability, it was difficult to catch a sustained ferroresonance at C_0 = 0.73 μF. In Fig. 20(d) a 50-Hz FR process has appeared after the second event and was interrupted by the third SLG. All other computed events were followed by chaotic processes, some of which evolved into normal oscillations.

The measured and computed processes in Fig. 20 illustrate the fact that, with everything else being equal, the type of FR oscillations depends on the fault clearance instant and may be different. Small discrepancies between modeled and measured waveforms in Figs. 18 to 20 may be ascribed to non-ideal voltage waveforms of the three-phase source employed in experiments and, probably, to non-identities of the used VTs.

5. Possibilities of simplified VT models

The use of the composite DHM facilitates the assessment of the effects of core losses and static hysteresis. By nullifying the dynamic loss coefficient of the DHM, this model is reduced to a static hysteresis model (SHM), and the full (DHM-based) VT model developed is reduced to a SHM-based model. The result of this simplification is that the number of envelope peaks becomes slightly less than that observed in the experiment (see Figs. 1(a) and 13). To restore the calculated picture, the values of L_{12} and L_{02} should be slightly increased. Corresponding values are indicated in the row "SHM-based" of Table 2.

The next simplification is to represent the core material by only a single-valued (anhysteretic) curve with no loss resistances in parallel to static nonlinear inductors of the leg and yoke. In order to maintain the accuracy achieved by the DHM-based model, inductances L_{12} and L_{02} of VT models have to be increased a little more. Their values are indicated in row "Lossless" of Table 2.

Such a lossless core representation is highly idealized, but the corresponding VT model is the easiest for implementation and computation. Using inductance values provided in Table 2, the network behaviors predicted by the SHM-based and lossless VT models practically coincide with those computed with the full DHM-based model.

6. Concluding remarks

The voltage transformer is always considered to be an element, whose model is crucial for studying network resonance behavior. In spite of trustworthy analytical tools developed to date, impacts of several transformer characteristics are studied numerically in different combinations in the growing ferroresonance literature. Among them, the core saturation is recognized as the most important factor. In addition, hysteretic properties of the core material and nonlinear dependencies of transformer losses on the operation frequency and the instant flux density are also identified as influential characteristics. When modeling complex ferroresonance transients recorded in dedicated experiments [9], it would be difficult to study the influence of these factors in isolation from each other. So, the authors decided to use first a Dynamic Hysteresis Model (DHM) recently included into the ATP/ATPDraw library. In addition to its quasi-static properties and dynamic extension, this catalog-based model is capable of reproducing *B-H* trajectories of typical grain-oriented steels in deep saturation. After fitting the network model for one of its capacitances, predictive validity of the model was confirmed for all other capacitances and thus ferroresonance modes observed in experiments.

It is shown that networks prone to *parallel* ferroresonance can be initially examined with the simplified lossless model, while the full VT model should be used for verification purposes.

The precision achieved in the modeling can help reduce costly mandatory measurements carried out over a wide range of the network's zero sequence capacitances [9]. Since with a known transformer design, the calculation of leakage parameters (inductances L_{12} and L_{02}) is a well-developed procedure, the proposed approach can be extended to cover other types of voltage transformers, in particular, new anti-ferroresonance measuring VTs, which are of primary consumer needs.

CRediT authorship contribution statement

S.E. Zirka: Conceptualization, Methodology, Writing - original draft. **Y.I. Moroz:** Software. **A.V. Zhuykov:** Investigation, Supervision. **D.A. Matveev:** . **M.A. Kubatkin:** Validation. **M.V. Frolov:** Methodology, Writing - review & editing. **M. Popov:** Investigation.

Declaration of Competing Interest

The authors declare that they have no known competing financial interests or personal relationships that could have appeared to influence the work reported in this paper.

References

[1] Iravani MR, Chaudhary AKS, Giesbrecht WJ, Hassan IE, Keri AJF, Lee KC, et al. Parameter determination for modeling system transients – Part III: Transformers. IEEE Trans Power Deliv 2000;15(1):255–65. https://doi.org/10.1109/61.847260.
[2] Shott HS, Peterson HA. Criteria for neutral stability of wye-grounded-primary broken-delta-secondary transformer circuits. Trans AIEE 1941;60:997–1002.
[3] Resonance and ferroresonance in power networks. CIGRE WG C4.307, ISBN: 978-2-85873-264-7,2014.
[4] Janssens N, Van Craenenbroeck T, Van Dommelen D, Van De Meulebroeke F. Direct calculation of the stability domains of three-phase ferroresonance in isolated neutral networks with grounded-neutral voltage transformers. IEEE Trans Power Deliv 1996;11(3):1546–53. https://doi.org/10.1109/61.517515.
[5] Piasecki W, Florkowski M, Fulczyk M, Mahonen P, Nowak W. Mitigating ferroresonance in voltage transformers in ungrounded MV networks. IEEE Trans Power Deliv 2007;22(4):2362–9. https://doi.org/10.1109/TPWRD.2007.905383.
[6] Fulchiron D. Basic selection of MV public distribution networks. Cahier technique no. 203, Schneider Electric: 2001.
[7] Saenko YL, Popov AS. Effectiveness of antiresonant voltage transformer insulation monitoring in networks with isolated neutral. Electrification Transport 2012;4:38–43. https://doi.org/10.15802/etr.v0i4.18051 [in Russian].
[8] IEC 61869-3:2012. Instrument transformers. – Part 3: Additional requirements for inductive voltage transformers.
[9] Zhuykov AV, Kubatkin MA, Matveev DA, Nikulov II, Frolov MV. Checking the anti-resonance properties of voltage transformers using the 6–35 kV experimental test bench in the context of the new standard requirements. Energetic 2019;10:46–52 [in Russian].
[10] Tokić A, Kasumović M, Demirović D, Turković I. Ferroresonance in 35 kV isolated networks: causes and mitigations. Elektrotehniski Vestnic/Electrotechnical Review 2016;83(5):259–65.
[11] Martínez R, Manana M, van Rodríguez JI, Álvarez M, et al. Ferroresonance phenomena in medium voltage isolated neutral grids: a case study. IET Renew. Power Gener 2019;13(1):209–14. https://doi.org/10.1049/iet-rpg.2018.5231.

[12] Solak K, Rebizant W, Kereit M. Detection of ferroresonance oscillations in medium voltage networks. Energies 2020;13:4129. https://doi.org/10.3390/en13164129.
[13] Stipetić N, Filipović-Grčić Božidar, Uglešić I, Xémard A, Andres N. Earth-fault detection and localization in isolated industrial MV network – comparison of directional overcurrent protection and signal injection method. Electr Power Syst Res. 2021;197(107313). https://doi.org/10.1016/j.epsr.2021.107313.
[14] Int. Standard IEC 60076-6: 2007 Power transformers, Part 6 – Reactors: Clause 10: Earthing transformer (neutral couplers).
[15] Belchior FN, Ferreira JFV, Oliveira JC, Apolonio R, Vasconcellos AB. Three-phase electromagnetic filter for zero-sequence harmonics. IEEE Trans Magn 2006;42(9): 2201–7. https://doi.org/10.1109/TMAG.2006.880398.
[16] Rezaei-Zare A, Iravani R, Sanaye-Pasand M, Mohseni H, Farhangi S. An accurate hysteresis model for ferroresonance analysis of a transformer. IEEE Trans Power Deliv 2008;23(3):1448–56. https://doi.org/10.1109/TPWRD.2007.916225.
[17] Moses P, Masoum MAS, Toliyat HA. Impact of hysteresis and magnetic couplings on the stability domain of ferroresonance in asymmetric three-phase three-leg transformers. IEEE Trans Energy Conv 2011;26(2):581–92. https://doi.org/10.1109/TEC.2010.2088400.
[18] Rezaei-Zare A, Sanaye-Pasand M, Mohseni H, Farhangi S, Iravani R. Analysis of ferroresonance modes in power transformers using Preisach-type hysteretic magnetizing inductance. IEEE Trans Power Deliv 2007;22(2):919–29. https://doi.org/10.1109/TPWRD.2006.877078.
[19] Rezaei-Zare A. Enhanced transformer model for low- and mid-frequency transients—Part II: Validation and simulation results. IEEE Trans Power Deliv 2015;30(1):316–25. https://doi.org/10.1109/TPWRD.2014.2347934.
[20] Corea-Araujo JA, González-Molina F, Martínez JA, Castro-Aranda F, Barrado-Rodrigo JA, et al. Single-phase transformer model validation for ferroresonance analysis including hysteresis. In: 2015 IEEE Power & Energy Society General Meeting, Denver, CO, USA, 2015, p. 1–5, doi: 10.1109/PESGM.2015.7285872.
[21] Emin Z, Yu KT. Ferroresonance experience in UK: Simulations and measurements. In: Int. conf. power systems transients, Rio de Janeiro, Brazil; 2001.
[22] Javora R, Iwahara M, Yamada S. Effect of dynamic core losses on ferroresonance phenomena. J. Mat Processing Tech 2005;161:156–61. https://doi.org/10.1016/j.jmatprotec.2004.07.019.
[23] Jacobson DAN, Menzies RW. Investigation of station service transformer ferroresonance in Manitoba Hydro's 230-kV Dorsey converter station. In: Int. conf. power systems transients, Rio de Janeiro, Brazil; 2001.
[24] Prusty S, Sanyal SK. Effect of core loss on multimodal operation of a parallel ferroresonant circuit: some generalised conclusions. Proc. IEE. 1979;126(9): 826–32. https://doi.org/10.1049/piee.1979.0257.
[25] Zirka SE, Moroz YI, Høidalen HK, Lotfi A, Chiesa N, Arturi CM. Practical experience in using a topological model of a core-type three-phase transformer—No-load and inrush conditions. IEEE Trans Power Deliv 2017;32(4):2081–90. https://doi.org/10.1109/TPWRD.2016.2618900.
[26] Zirka SE, Moroz YI, Chiesa N, Harrison RG, Hoidalen HKr. Implementation of inverse hysteresis model into EMTP – Part II: Dynamic model. IEEE Trans Power Deliv 2015;30(5):2233–41. https://doi.org/10.1109/TPWRD.2015.2416199.
[27] Bykova AM, Zhuykov AV, Konstantinova AY, Kubatkin MA, Matveev DA, Nikulov II. Application of neutral forming filters FMZO for resonant and resistive neutral grounding. Energetic 2019;10:26–9 [in Russian].
[28] Martinez-Velasco JA, Gonzalez-Molina F. Calculation of power system overvoltages. In: Martinez-Velasco JA. editor. Transient analysis of power systems. John Wiley & Sons; 2015.
[29] Zhao J, Zirka SE, Moroz YI, Arturi CM. Structure and properties of the hybrid and topological transformer models. Electr Power Energy Syst 2020;118:105785. https://doi.org/10.1016/j.ijepes.2019.105785.
[30] Zirka SE, Moroz YI, Arturi CM, Chiesa N, Høidalen HK. Topology-correct reversible transformer model. IEEE Trans Power Deliv 2012;27(4):2037–45. https://doi.org/10.1109/TPWRD.2012.2205275.
[31] de León F, Farazmand A, Joseph P. Comparing the T and π equivalent circuits for the calculation of transformer inrush currents. IEEE Trans Power Deliv 2012;27(4): 2390–8. https://doi.org/10.1109/TPWRD.2012.2208229.
[32] Chiesa N, Mork BA, Høidalen HK. Transformer model for inrush current calculations: Simulations, measurements and sensitivity analysis. IEEE Trans Power Deliv 2010;25(4):2599–608. https://doi.org/10.1109/TPWRD.2010.2045518.
[33] Lur'e AI. Transformer connection under no-load and short-circuit events. Russian Elect Eng 2008;79(2):57–70. https://doi.org/10.3103/S1068371208020016.
[34] Armco oriented and Tran-Cor H electrical steels. Armco Inc., Middletown, Ohio; 1979.
[35] Yang M, Sima W, Yang Q, Li J, Zou M, Duan Q. Non-linear characteristic quantity extraction of ferroresonance overvoltage time series. IET Gener. Transm Dis 2017; 11(6):1427–33. https://doi.org/10.1049/iet-gtd.2016.0873.
[36] Høidalen HK, Mork BA, Gonzalez F, Ishchenko D, Chiesa N. Implementation and verification of the Hybrid Transformer model in ATPDraw. Electr Power Syst Res 2009;79:454–9. https://doi.org/10.1016/j.epsr.2008.09.003.
[37] Vavin VN. Voltage transformers and their secondary circuits. Moscow: Energiya; 1977 [in Russian].
[38] Zikherman MKh. Magnetizing characteristics of large power transformers. Elektrichestvo 1972;3:79–82 [in Russian].
[40] Prikler L, Kizilcay M, Bán G, Handl P. Improved secondary arc models based on identification of arc parameters from staged fault test records. In: 14th Power Syst Comp Conf, Sevilla, Spain; 2002.

Further reading

[39] Dommel HW, et al. Electromagnetic Transients Program Reference Manual (EMTP Theory Book). Portland, OR: Prepared for BPA; 1986.